

The crossing LCL domains of the IR dimer are represented here only in their general shape (Fig. 4, B and C); the known x-ray coordinates are not yet available (5). Nonetheless, the slightly asymmetric NGBI location indicated that one insulin molecule contacts the L1-Cys-rich domains of one α subunit and the L2 domain of the other α subunit. A theoretical model involving both α subunits in the high-affinity insulin binding has previously been proposed (16). Our 3D reconstruction provides structural evidence for this mode of binding, for the bivalency of the IR, and for structural interaction of the two binding sites. This explains the curvilinear Scatchard plot, the negative cooperativity of insulin binding (17), and the low-affinity binding of IR monomers (18).

Monomeric inactive receptor TKs, such as the epidermal growth factor receptor and platelet-derived growth factor receptor, are dimerized and activated by ligand binding (19). In the intrinsically dimeric IR family receptors, the distance between the two cytoplasmic β -subunit TKs must be too great for activation without ligand binding. Hubbard *et al.* (4) suggested that insulin binding to IR decreased this distance by disengaging Tyr¹¹⁶² from the catalytic loop. In our reconstruction of IR bound to a single NGBI, a good fit to the ligand-receptor complex is obtained when the two TK domains are oriented with their catalytic loops juxtaposed. An extended flexible activation loop of TK, which moves 30 Å between the inactive and activated states ascertained crystallographically (4), can just reach the catalytic loop of the opposing TK. Thus, one molecule of insulin is sufficient to bring the IR to an activating configuration.

The 3D quaternary structure of the IR-insulin complex, formed in the absence of ATP, likely represents an intermediate state between insulin-free IR and the fully activated, phosphorylated IR. In the absence of a crystallographic structure of the entire insulin receptor, the 3D reconstruction provides structural information toward the full understanding of transmembrane signal transmission in insulin action. This 3D reconstruction approach may be applicable to determining the quaternary structure of other large protein complexes that are refractory to crystallization.

References and Notes

1. M. Bajaj, M. D. Waterfield, J. Schlessinger, W. R. Taylor, T. Blundell, *Biochim. Biophys. Acta* **916**, 220 (1987).
2. A. Ullrich and J. Schlessinger, *Cell* **61**, 203 (1990).
3. M. R. White and R. Kahn, *J. Biol. Chem.* **269**, 1 (1994).
4. S. R. Hubbard, L. Wei, L. Ellis, W. A. Hendrickson, *Nature* **372**, 746 (1994); S. R. Hubbard, *EMBO J.* **16**, 5572 (1997).
5. T. P. J. Garrett *et al.*, *Nature* **394**, 395 (1998).
6. J. P. O'Bryan *et al.*, *Mol. Cell. Biol.* **11**, 5016 (1991); E. B. Pasquale, *Cell Recognition* **2**, 523 (1991).
7. Bis-(t-Boc)-bovine-insulin (BBI) was prepared as described [R. Geiger, H. H. Schöne, W. Pfaff, *Physiol. Chem.* **352**, 1487 (1971)]. BBI (1 mg) and mono-NHS-Nanogold (30 nmol) (Nanoprobes, Stony-

brook, NY) were dissolved in 200 μ l of *N,N*-dimethylacetamide containing 2 μ l of di-isopropylethylamine, pH 7.6. After vigorous mixing at room temperature for 60 min the mixture was vacuum dried. The pellet obtained was dissolved in 20 μ l of trifluoroacetic acid, kept at room temperature for 5 min, and then dried again. The pellet, resuspended in 120 μ l of 1 M acetic acid, was chromatographed twice on a BioGel P10 column (1.7 cm by 25 cm) in 1 M acetic acid. The NGBI, >95% pure, had a molecular mass of 19,796 daltons by matrix-assisted laser desorption/ionization (MALDI) time-of-flight (TOF) mass spectrometry (Fig. 1, inset), consistent with one insulin per Nanogold cluster.

8. J. Murray-Rust, A. N. McLeod, T. L. Blundell, S. P. Wood, *BioAssay* **14**, 325 (1992).
9. Y. Fujita-Yamaguchi, S. Choi, Y. Sakamoto, K. Itakura, *J. Biol. Chem.* **258**, 5045 (1983).
10. IR protein was solubilized from human placental membranes and purified by affinity chromatography on an insulin column (9), followed by fast protein liquid chromatography purification on Sephacryl S200. The IR was greater than 95% pure by SDS-polyacrylamide gel electrophoresis (SDS-PAGE) (10%) and Coomassie staining. IR ($\sim 0.5 \times 10^{-7}$ M) was incubated with NGBI ($\sim 0.5 \times 10^{-6}$ M) at 4°C overnight in 20 mM HEPES buffer (pH 7.5). Unbound NGBI was removed by microfiltration with a size cut-off of 300 kD (Sigma). The mixture was diluted to 7.5 μ g of receptor protein per milliliter in 20 mM HEPES buffer (pH 7.5) for STEM.
11. The specimen (5 μ l) was injected into 5 μ l of the HEPES buffer on a grid overlaid with a 23 Å carbon film on fenestrated celluloseacetobutylate, then washed with HEPES buffer and 10 mM ammonium acetate (pH 7.5). The grid was wicked with filter paper, leaving a very thin solution layer, then quick-frozen in liquid ethane at -150°C . The frozen specimen was transferred at below -140°C into the STEM (Vacuum Generators, Model HB601UX) cold-stage and freeze-dried at -140°C . We acquired simultaneous elastic and inelastic digital images with 6.5 Å pixels using single-electron counting at 100 kV, with the specimen at -150°C . The beam size was 3 Å.
12. Paired elastic and inelastic images were combined for a fourfold signal increase over the elastic signal alone for carbonaceous specimens [R. F. Egerton, *Electron Energy-Loss Spectroscopy in the Electron Microscope*

(Plenum, New York, ed. 2, 1996), p. 145]. Single particles were interactively selected and low-pass filtered to 1.0 nm with a Gaussian filter with the programs WEB and SPIDER (Wadsworth Laboratories, Albany, NY). The molecular mass relative to the 23 Å carbon support had a Gaussian distribution with a modal mass of 570 kD, including 480 kD for the IR-NGBI plus ~ 150 Triton X100 molecules. We computed orientations and 3D reconstructions as before [N. A. Farrow and F. P. Ottensmeyer, *J. Opt. Soc. Am.* **A9**, 1749 (1992); *Ultramicroscopy* **52**, 141 (1993)] on an SGI Indigo workstation (Silicon Graphics, Mountain View, CA) using filtered back-projection and an angular distribution-dependent filter. Resolution measurements were obtained by means of Fourier shell-phase residual calculations between reconstructions from two independent sets of half of the 704 images [G. J. Czarnota, D. W. Andrews, N. A. Farrow, F. P. Ottensmeyer, *J. Struct. Biol.* **113**, 35 (1994)]. INSIGHT II (Molecular Simulations, San Diego, CA) served to insert known crystal structures and approximate models. Handedness was determined by fitting the crystallographic structure of TK into mirror pairs of the reconstruction.

13. M. Fabry *et al.*, *J. Biol. Chem.* **267**, 8950 (1992).
14. T. D. Mulhern, G. W. Booker, L. Cosgrove, *Trends Biochem. Sci.* **23**, 465 (1998).
15. C. C. Yip, *J. Cell. Biochem.* **48**, 19 (1992); L. Schäffer, *Exp. Clin. Endocrinol.* **101**, 7 (1993); P. De Meyts *et al.*, *ibid.*, p. 17.
16. P. De Meyts, A. R. Bianco, J. Roth, *J. Biol. Chem.* **251**, 1877 (1976).
17. M. Boni-Schnetzler *et al.*, *ibid.* **262**, 8395 (1987); L. J. Sweet, B. D. Morrison, J. E. Pessin, *ibid.*, p. 6939.
18. F. Canals, *Biochemistry* **31**, 4493 (1992); J. Schlessinger and A. Ullrich, *Neuron* **9**, 383 (1992).
19. C. Christensen, F. C. Wiberg, L. Schäffer, A. S. Anderson, *J. Biol. Chem.* **273**, 17780 (1998).
20. Y. Ebina *et al.*, *Cell* **40**, 747 (1985).
21. G. D. Smith, E. Ciszak, W. Pangborn, *Protein Sci.* **5**, 1502 (1996).
22. We thank Y. Mao, M. Burke, B. Rutherford, and H. Hsu for their technical assistance. Supported by grants from the Medical Research Council of Canada, the National Cancer Institute of Canada, and by funds from Cancer Care Ontario.

26 March 1999; accepted 14 July 1999

Coordinate Regulation of RAG1 and RAG2 by Cell Type-Specific DNA Elements 5' of RAG2

Wong Yu,¹ Ziva Misulovin,² Heikyung Suh,² Richard R. Hardy,³ Mila Jankovic,¹ Nikos Yannoutsos,¹ Michel C. Nussenzweig^{2*}

RAG1 and RAG2 are essential for V(D)J recombination and lymphocyte development. These genes are thought to encode a transposase derived from a mobile genetic element that was inserted into the vertebrate genome 450 million years ago. The regulation of RAG1 and RAG2 was investigated in vivo with bacterial artificial chromosome (BAC) transgenes containing a fluorescent indicator. Coordinate expression of RAG1 and RAG2 in B and T cells was found to be regulated by distinct genetic elements found on the 5' side of the RAG2 gene. This observation suggests a mechanism by which asymmetrically disposed cis DNA elements could influence the expression of the primordial transposon and thereby capture RAGs for vertebrate evolution.

Vertebrates assemble immunoglobulins (Igs) and T cell receptors (TCRs) by a site-specific DNA recombination reaction known as V(D)J recombination (1). V(D)J recombination occurs only in lymphocytes and is catalyzed by the

protein products of the recombinase-activating genes RAG1 and RAG2 (2). RAGs initiate V(D)J recombination by recognizing recombination signal sequences that flank Ig and TCR variable, diversity, and joining gene segments

REPORTS

(3). RAG-catalyzed DNA cleavage proceeds by a mechanism similar to bacterial Tn10 transposition (4). Like Tn10, RAGs nick double-stranded (ds) DNA (3) and then cleave the opposite strand by trans-esterification (5). The hairpin products of trans-esterification can then be opened by RAGs or Tn10 in a second DNA-nicking reaction (6, 7). Ubiquitous DNA ds-break repair factors, including Ku70 and 80, DNA-dependent protein kinase, XRCC4, and ligase IV, are required to repair the RAG-induced breaks and for normal lymphocyte development (8).

Coordinate expression of RAG1 and RAG2 is restricted to lymphocytes and is essential for lymphocyte development (2, 9). In the absence of either RAG1 or RAG2, B and T cell development is completely abrogated (9). Conversely, aberrant RAG expression results in abnormal lymphocyte development (10). Despite the central importance of regulated RAG expression in the development, evolution, and function of the immune system, little is known about the molecular mechanisms that control RAG transcription.

To examine the mechanisms that regulate RAG2 expression in vivo, we produced transgenic mice that carry bacterial artificial chromosomes (BACs) modified by homologous recombination to encode a green fluorescent protein (GFP) reporter instead of RAG2 (11, 12). Three overlapping BACs (NG, HG, and MG) that cover the RAG locus were obtained by screening libraries with oligonucleotides complementary to RAG1 (Fig. 1). The HG BAC was further modified by homologous

recombination to create additional BAC constructs (Fig. 1).

We first investigated whether GFP-containing BACs could direct proper transcriptional regulation of *RAG2* in lymphocytes by analyzing mice transgenic for the NG BAC, as the *RAG* coding regions were located centrally within this genomic insert (Fig. 1) (12). Bone marrow B cells were developmentally staged by cell surface markers and analyzed by flow cytometry (13) (Fig. 2A). Green fluorescence was detected in bone marrow fraction A1, which contains the most immature committed B cell precursors, and fluorescence increased in the pre-pro-B cell subpopulation, where V(D)J recombination is first detected (fraction A2) (13). RAG2-GFP expression peaked in pro-B cells that undergo immunoglobulin heavy chain D-J and V-DJ recombination (fractions B and C) and decreased in large cycling pre-B cells (fraction

C') (13, 14). Small pre-B cells undergoing light chain gene recombination also had high green fluorescence (fraction D) that disappeared in mature recirculating CD43⁻B220^{high} B cells (fraction F). This temporal pattern of RAG2-GFP expression matched reported endogenous *RAG2* expression (13, 14), and coordinate expression of RAG2-GFP mRNA and endogenous *RAG2* mRNA was confirmed (12, 15). Thus, NG BAC contained all cis elements necessary for the proper expression of *RAG2* mRNA in B cells.

Consistent with previous in situ work on endogenous *RAG* expression in the thymus, GFP expression was most prominent in the cortex, where immature CD4⁺CD8⁺ double-positive (DP) T cells undergo V(D)J recombination (Fig. 2B) (16). In contrast, the thymic medulla, which contains more mature T cells, was only weakly fluorescent.

Thymocytes were then analyzed by flow

¹Laboratory of Molecular Immunology, Rockefeller University, 1230 York Avenue, New York, NY 10021, USA. ²Howard Hughes Medical Institute, Laboratory of Molecular Immunology, Rockefeller University, 1230 York Avenue, New York, NY 10021, USA. ³Institute for Cancer Research, Fox Chase Cancer Center, Philadelphia, PA 19111, USA.

*To whom correspondence should be addressed. E-mail: nussen@rockvax.rockefeller.edu

Fig. 1. Diagram of BAC transgenes and summary of indicator expression in T cells and B cells. RAG2-GFP (12) and RAG1-YFP expression was detected by flow cytometry. To produce R1Δ, HGΔ, HGΔ2, and HGΔ3, HG was further modified by homologous recombination (26). HYG and HYGΔ were produced by inserting EYFP (Clontech) at the *RAG1* start codon of HG and HGΔ, respectively. HYG and HYGΔ were further modified to produce INSΔ and R2Δ, respectively (26). Symbols: *, RAG1-YFP or RAG2-GFP (or both) present at levels comparable to NG in DN but not in DP thymocytes (Fig. 2B); ^, RAG1-YFP present at low levels in developing B cells (See Fig. 4A) and DN thymocytes (27), but not in DP thymocytes.

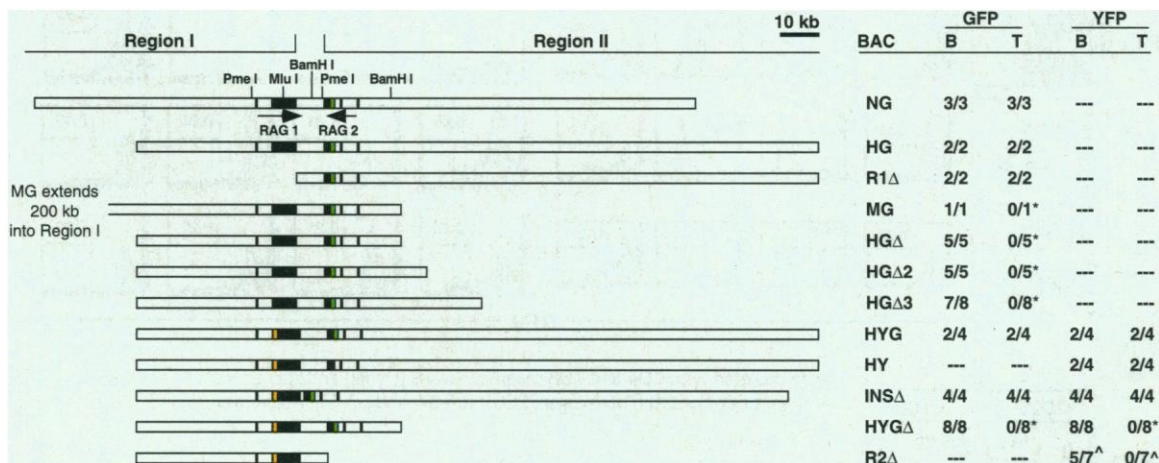
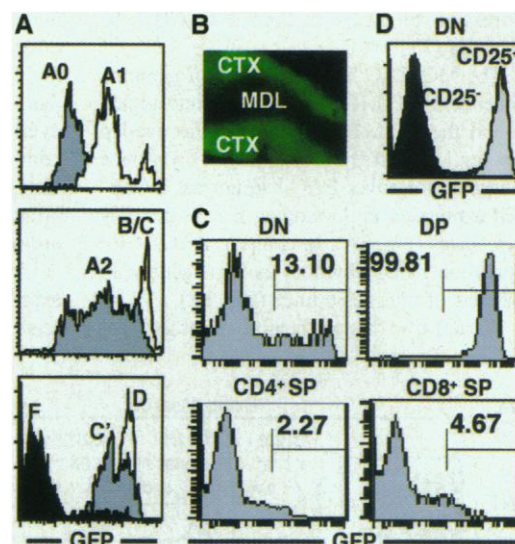


Fig. 2. GFP expression in the bone marrow, thymus, and spleen of NG transgenic mice. (A) Cytofluorographic analysis of GFP expression in developing B cells of NG transgenic mice. Histograms show GFP expression on gated fractions (13). (B) Confocal micrograph showing GFP expression in the thymus from an NG transgenic mouse. Thymic cortex (CTX) and medulla (MDL) are indicated. (C) Cytofluorographic analysis of GFP expression in T cells from thymus and spleen of NG transgenic mice. Histograms show GFP fluorescence in CD4⁻CD8⁻ DN and CD4⁺CD8⁺ DP thymocytes and in CD4⁻CD8⁻ and CD4⁻CD8⁺ SP splenocytes. Thymocytes and spleen cells were stained with phycoerythrin (PE) antibody to CD8 and biotin antibody to CD4 (Pharmin; 53-6.7 and RM4-4, respectively) developed with streptavidin red-670 (Gibco-BRL). (D) Histogram shows GFP expression in CD25⁺ or CD25⁻ DN thymocytes. APC-GK1.5 (antibody to CD4), APC-53-6.7 (antibody to CD8a), and BI-PC61 (antibody to CD25) followed by TR-Avidin and PI to label dead cells were used to visualize thymocyte DN subsets.



cytometry. Among CD4⁻CD8⁻ double-negative (DN) thymocytes, γ , δ , and β chain rearrangements are detected in the CD25⁺ subpopulation. Consistent with this, RAG2-GFP was expressed in the CD25⁺ subset of DN thymocytes (Fig. 2, C and D). DP thymocytes were fluorescent, but mature CD4⁺CD8⁻ or CD4⁻CD8⁺ single-positive (SP) T cells in the spleen were not (Fig. 2C) (15). Thus, the NG BAC contained all cis elements necessary for regulated transcription of RAG2 in T cells as well as in B cells (17).

Two additional BAC constructs, HG and R1 Δ (Fig. 1), also directed proper RAG2 transcription in T and B cells (Fig. 3A); that is, the pattern of expression was the same as in NG BAC transgenic mice. As judged by the overlap between the NG, HG, and R1 Δ BACs, region I is not required for regulated RAG2 expression in T or B cells (Fig. 1). Thus, the 100-kb genomic overlap between NG and R1 Δ is sufficient to direct regulated expression of RAG2 in both T and B cells (Fig. 1) (17).

The MG BAC has only 10 kb of genomic sequence 5' of RAG2 that extends into region II, and the HG Δ BAC has only the overlap between MG and HG BACs (Fig. 1), yet mice transgenic for either BAC had normal RAG2-GFP expression in developing B cells and DN thymocytes (Fig. 3A). In contrast, RAG2-GFP expression in DP thymocytes was reduced in both sets of transgenic mice (Fig. 3A).

To narrow the cis region necessary for

RAG2 expression in DP thymocytes, we created the HG Δ 2 and HG Δ 3 BACs, which contain genomic sequences extending an additional 5.5 kb and 19.5 kb, respectively, into region II as compared with HG Δ (Fig. 1). HG Δ 2 and HG Δ 3 transgenic mice resembled HG Δ transgenic mice in that GFP fluorescence was found in developing B cells and DN thymocytes, but not in DP thymocytes (Fig. 1). Thus, the DNA sequences required to direct fully regulated expression of RAG2 in DP thymocytes are found in a 55-kb interval between the ends of BACs HG Δ 3 and NG in region II (Fig. 1).

To determine whether RAG2 expression in DN thymocytes in HG Δ transgenic mice was properly regulated as in B cells, we subfractionated these cells according to CD25 expression. As in NG mice, CD25⁺ DN thymocytes from HG Δ mice expressed RAG2-GFP and CD25⁻ cells did not (Figs. 2D and 3B). Thus, RAG2 was properly regulated in DN thymocytes in HG Δ transgenic mice, and expression of RAG2 in DN and DP thymocytes can be dissociated. We conclude that the 23 kb of sequence found in the overlap between R1 Δ and HG Δ BACs contains sufficient information to direct expression of R2-GFP in a developmentally appropriate fashion in B cells and DN T cells but not in DP T cells.

A pattern of greatly reduced RAG2-GFP expression in DP thymocytes coupled with relatively normal GFP levels in DN thymo-

cytes and B cells was observed in 18 of 19 independent founders transgenic for the MG, HG Δ , HG Δ 2, or HG Δ 3 BACs (Fig. 1). This abnormal pattern of RAG2 expression suggests the existence of proximal elements, which contribute to, but cannot fully direct, T cell expression of RAG2. Consistent with this, the human and mouse RAG1 and RAG2 promoters have basal transcriptional activity (18). In particular, in vitro experiments indicate that the murine RAG2 promoter has lymphoid specificity and is regulated differently in T and B cells (18). We conclude that a promoter distal element or elements in region II likely interact with more proximal elements to confer complete transcriptional regulation of RAG2 (19).

To examine the regulation of RAG1 in vivo and to determine whether RAG1 and RAG2 are coordinately expressed, we created the HYG BAC by inserting a yellow fluorescence protein (YFP) indicator into the RAG1 gene of the HG BAC (Fig. 1). Four lines of transgenic mice that carry HYG were analyzed; two of the four lines expressed both genes and two lines expressed neither (Fig. 1). In both expressing lines, B and T cells displayed a broader distribution of yellow than green fluorescence (Fig. 4A). Nevertheless, RAG1-YFP and RAG2-GFP expression were coordinate, and their temporal regulation was indistinguishable from that shown when RAG2 was assayed alone in HG transgenic mice (Figs. 1 and 4A) (20). Deletion of the

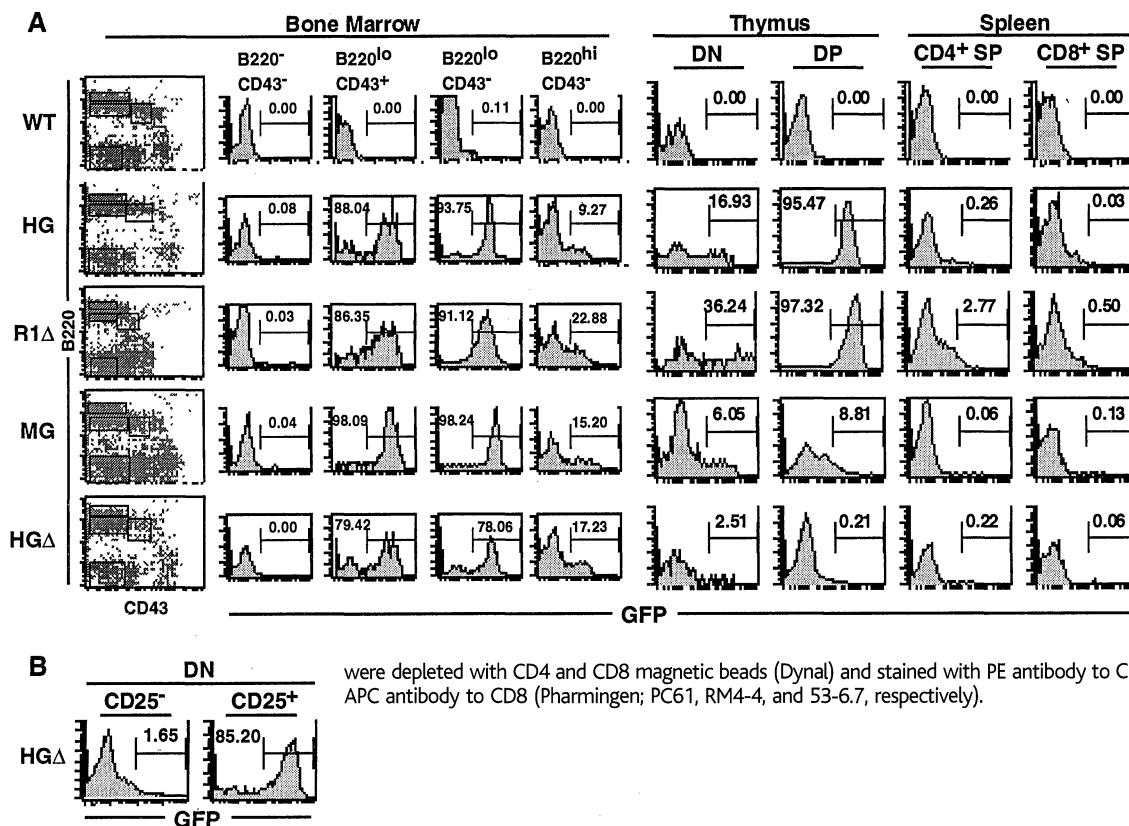


Fig. 3. RAG2-GFP expression in mice transgenic for modified BACs. (A) (Left) Histograms show GFP expression in bone marrow cells electronically gated on the basis of PE antibody to B220 and biotin antibody to CD43 staining (Pharmingen; RA3-6B2 and S7, respectively, developed with streptavidin red-670). (Right) Histograms show GFP expression in T cells from thymus and spleen gated as indicated. WT, wild type; DN, CD4⁻CD8⁻ double negative; DP, CD4⁺CD8⁺ double positive. (B) RAG2-GFP expression in HG Δ DN thymocytes. Histograms show GFP expression in electronically gated CD25⁺ or CD25⁻ DN thymocytes. DP and SP thymocytes

were depleted with CD4 and CD8 magnetic beads (Dynal) and stained with PE antibody to CD25, APC antibody to CD4, and APC antibody to CD8 (Pharmingen; PC61, RM4-4, and 53-6.7, respectively).

intergenic sequence between *RAG1* and *RAG2* did not alter the pattern of expression of either *RAG1*-YFP or *RAG2*-GFP (INS Δ , Fig. 1). Thus, the intergenic sequence was not essential for regulation of either *RAG1* or *RAG2*, and the HYG BAC carries sufficient information to direct the expression of *RAG1* and *RAG2* in B cells and T cells in a developmentally regulated and coordinate fashion.

To explore the cis requirements for *RAG1* expression in T cells, we generated the HYG Δ BAC by inserting YFP into the start codon of *RAG1* in HG Δ (Figs. 1 and 4A). HYG Δ directed coordinate expression of *RAG1*-YFP and *RAG2*-GFP in developing B cells (Fig. 4A) and DN thymocytes (Fig. 1), and, again, there was a broader distribution of YFP fluorescence than GFP fluorescence. In contrast, neither YFP nor GFP was expressed in DP thymocytes in the eight transgenic HYG Δ founders (Fig. 1). Thus, the 105-kb genomic interval in region II between the ends of HYG Δ BAC and the HYG BAC is essential for regulated expression of *RAG1* in DP thymocytes, but not in DN thymocytes or B cells (Fig. 1). Expression of *RAG1* in DP thymocytes, therefore, requires DNA elements found on the *RAG2* side of the locus.

To determine whether the cis elements required for regulated expression of *RAG1* in B cells and DN T cells are on the *RAG1* or *RAG2* side of the RAG locus, we removed sequences in region II from the HYG Δ BAC to create the R2 Δ BAC (Figs. 1 and 4A). In five of the seven R2 Δ founders, low yellow fluorescence was detected in pro- and pre-B cells and in DN thymocytes (Figs. 1 and 4A) (21), indicating that elements on the *RAG1* side of the locus contribute to regulation of *RAG1* in these cells (18) but that these elements are not sufficient for high expression of *RAG1*. In contrast to B cells and DN

thymocytes, *RAG1*-YFP was not detectable in DP thymocytes in R2 Δ transgenic mice (Fig. 1) (21). We conclude that both *RAG1* and *RAG2* are in part regulated by cis elements located 5' of *RAG2* in region II.

RAG1 and *RAG2* are unusual genes. They have remained closely linked and convergently transcribed throughout vertebrate evolution and have similarities to transposases (2, 22), including in vitro transposase activity (23). This led to the proposal that *RAG1* and *RAG2* entered the vertebrate genome as a mobile genetic element (2) and that transposase target sequences were inserted into a primordial receptor gene to create the first split antigen receptor gene (23, 24). The finding that *RAG1* and *RAG2* are coordinately regulated by asymmetrically disposed elements supports this hypothesis and suggests that the original integration may have occurred at a site where elements on one side of the transposon were able to influence the expression of both *RAG* genes coordinately. Lymphoid specificity may have been added after primordial transposition.

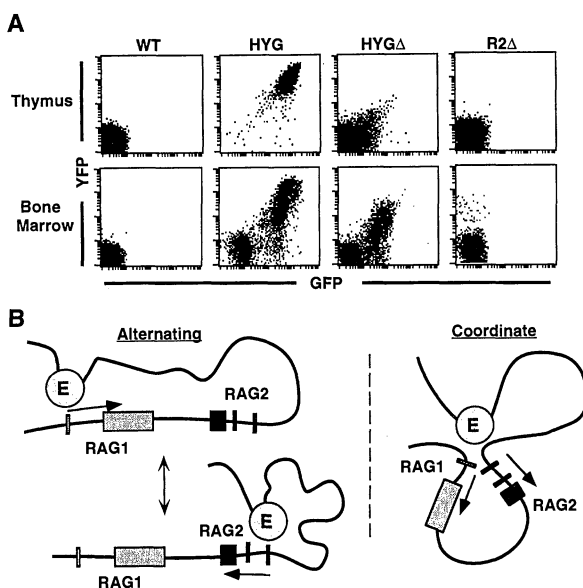
How can a set of elements on the *RAG2* side of the RAG locus control transcription of both *RAG1* and *RAG2*? One possibility is that elements on the *RAG2* side of the locus alternately loop between the *RAG1* and *RAG2* promoters by a switching mechanism similar to that of the human β globin locus (25). Such a switching model would require that *RAGs* remained linked but would not explain why they remained in a convergent transcriptional orientation (Fig. 4B). A second possibility is that the regulatory elements in region II loop to interact with both *RAG1* and *RAG2* promoters simultaneously (Fig. 4B). DNA looping to coordinate transcription would require that *RAG1* and *RAG2* remain closely linked in the genome, would

allow for separate transcriptional control in T and B cells, and might favor conservation of the original convergent orientation of *RAG1* and *RAG2*.

References and Notes

1. S. Tonegawa, *Nature* **302**, 575 (1983).
2. D. G. Schatz *et al.*, *Cell* **59**, 1035 (1989); M. A. Oettinger *et al.*, *Science* **248**, 1517 (1990); M. A. Oettinger *et al.*, *Immunogenetics* **35**, 97 (1992).
3. J. F. McLane *et al.*, *Cell* **83**, 387 (1995).
4. A. K. Kennedy *et al.*, *ibid.* **95**, 125 (1998).
5. D. C. van Gent *et al.*, *Science* **271**, 1592 (1996).
6. E. Besmer *et al.*, *Mol. Cell* **2**, 817 (1998).
7. P. E. Shockett and D. G. Schatz, *Mol. Cell Biol.* **19**, 4159 (1999).
8. T. Blunt *et al.*, *Cell* **80**, 813 (1995); C. U. Kirchgesner *et al.*, *Science* **267**, 1178 (1995); A. Nussenzweig *et al.*, *Nature* **382**, 551 (1996); C. Zhu *et al.*, *Cell* **86**, 379 (1996); H. Ouyang *et al.*, *J. Exp. Med.* **186**, 921 (1997); Y. Gu *et al.*, *Immunity* **7**, 653 (1997); U. Grawunder *et al.*, *Mol. Cell* **2**, 477 (1998); K. M. Frank *et al.*, *Nature* **396**, 173 (1998); Y. Gao *et al.*, *Cell* **95**, 891 (1998).
9. Y. Shinkai *et al.*, *Cell* **68**, 855 (1992); P. Mombaerts *et al.*, *ibid.*, p. 869.
10. J. Wayne *et al.*, *Immunity* **1**, 95 (1994).
11. X. W. Yang, P. Model, N. Heintz, *Nature Biotechnol.* **15**, 859 (1997).
12. Y. Wong *et al.*, *Nature*, in press.
13. L. Yue-Sheng *et al.*, *Immunity* **5**, 527 (1996); D. Allman *et al.*, *J. Exp. Med.* **189**, 735 (1999).
14. U. Grawunder *et al.*, *Immunity* **3**, 601 (1995).
15. The degradation of both GFP and *RAG2* protein lags behind that of *RAG2*-GFP and endogenous *RAG2* mRNA in fraction E immature B cells. Residual green fluorescence also persists in SP thymocytes that contain neither *RAG2*-GFP mRNA nor endogenous *RAG2* mRNA. Thus, green fluorescence indicates recent *RAG2* mRNA expression but is not a quantitative measure of *RAG2* mRNA levels (12).
16. L. A. Turka *et al.*, *Science* **253**, 778 (1991).
17. The transgene copy number in three NG, two HG, and two R1 Δ mouse lines ranged from 2 to 8, and higher copy number correlated with higher intensity GFP fluorescence.
18. T. Kitagawa *et al.*, *Blood* **88**, 3785 (1996); H. Kurioka *et al.*, *Mol. Immunol.* **33**, 1059 (1996); S. T. Brown *et al.*, *J. Immunol.* **158**, 5071 (1997); K. Fuller and U. Storb, *Mol. Immunol.* **34**, 939 (1997); A. A. Zarrin, I. Fong, L. Malkin, P. A. Marsden, N. L. Berenstein, *J. Immunol.* **159**, 4381 (1997); J. Lauring and M. S. Schlissel, *Mol. Cell Biol.* **19**, 2601 (1999).
19. The existence of promoter proximal elements that contribute to regulated *RAG2* expression is further supported by results from six independent founder mice transgenic for a genomic 17-kb Bam HI fragment that flanks the *RAG2* gene (2). Developmentally regulated *RAG2* expression was found in a variable fraction of pre-B cells and thymocytes in these lines. Therefore, some of the elements that direct *RAG2* in these cells must be in this 17-kb fragment, and the absence of T cell expression in larger fragments may in part be due to cell type-specific suppressors.
20. Insertion of YFP into the *RAG1* gene produced variable degrees of variegation of *RAG2*-GFP and *RAG1*-YFP expression in developing T and B cells [S. Henikoff, *Bioessays* **18**, 401 (1996); D. Kioussis and R. Festenstein, *Curr. Opin. Genet. Dev.* **7**, 614 (1997)]. Variegation was also observed in the absence of GFP when YFP alone was inserted into the *RAG1* start codon of the full-length H-BAC. Transgenic lines were defined as variegating when less than 70% of the DP thymocytes or pre-B cells were GFP positive.
21. Data can be found in Web Fig. 1 at <http://www.sciencemag.org/feature/data/1041564.shl>.
22. S. M. Lewis and G. E. Wu, *Cell* **88**, 159 (1997).
23. A. Agrawal *et al.*, *Nature* **394**, 744 (1998); K. Hiom *et al.*, *Cell* **94**, 463 (1998).
24. C. B. Thompson, *Immunity* **3**, 531 (1995).
25. M. Wijgerde *et al.*, *Nature* **377**, 209 (1995).
26. BACs were modified as described (17, 12). Shuttle vector inserts were constructed by PCR on an H-BAC template with the following sets of primer pairs: H

Fig. 4. Expression of *RAG1*-YFP and *RAG2*-GFP in mice transgenic for modified BACs. (A) Dot plots show YFP and GFP coexpression in bone marrow lymphocytes and thymocytes electronically gated on the basis of forward and side scatter. (B) Two models of transcriptional activation at the RAG locus. E, proposed cis regulatory element or elements.



deletion: 104, 5'-AGCAGACGAGTCGACAGCTCCAT-TAGCTTCCAGGTTTCG-3'; 105, 5'-GACCTGCAGAC-GGCTCCTCTGACCTACGAGTTCCACC-3'; 106, 5'-GT-CAGAGGACCGCTCTGCGAGTCTAGAGGATC-C-3'; 107, 5'-GACATCAGAGTCGACTGATGGCCTCCA-CGCACGTTGTG-3'; H deletion #2: 162, 5'-AGCAGA-CGAGTCGACGCTGGGCCAAGGAGTCAG-3'; 161, 5'-GTTGTAACGACGCGATCCAGACTCACATGGTCC-CTG-3'; 160, 5'-AGTCTGGGATCCGTCGTTTTACAA-CGTCGTGACTGGG-3'; 107, 5'-GACATCAGAGTCGA-CTGATGGCTCCACGACGTTGTG-3'; H deletion #3: 184, 5'-AGCAGACGAGTCGACAGCTGTGGTGATAGTA-TGAAGTATGAC-3'; 183, 5'-GTTGTAACGACGCTGA-GTTATGTAACAATCGAACG-3'; 182, 5'-ACATAACTAC-ACGTCGTTTTACAACGTCGTGACTGGG-3'; 107, 5'-G-ACATCAGAGTCGACTGATGGCTCCACGCACGTTGTG-3'; R1 deletion: 142, 5'-GGCAGTTATGGTGCCCT-TTAAACG-3'; 132, 5'-CAAATAGTACTATGCGTGTA-

ATGAAGCCAATGCTAAGTGG-3'; 124, 5'-GCTTCATT-TACACGCAATGTACTATTGTATTTGAGGACC-3'; 154, 5'-GACATCAGAGTCGACAACTCGAAGTAACAG-GTCAGAAAGC-3'; R1YFP: 5'sal/r1, 5'-AGCAGACGA-GTCGACACAACCAATCTCCCGAAGAATGC-3'; 3'r1/yfp, 5'-CTTGCTCACCATGGTTTTCTAAGCTACCTGGG-AACAATG-3'; 5'r1/yfp, 5'-GCTTAGCCACCATGGTG-AGCAAGGGCGAGC-3'; 3'yfp/r1, 5'-AAGGAGGCAG-CTTACTGTACAGCTCGTCCATGCC-3'; 5'yfp/r1, 5'-GCTGTACAAGTAAGCTGCCCTCTGCCCTACCC-3'; 3'r1/sal, 5'-GACATCAGAGTCGACGCTGTGG-GGGTGCCACTC-3'; R2 deletion: 129, 5'-AGCAGAC-GAGTCGACGGCAAGTCCATAGCATTACTTGG-3'; 130, 5'-GATATGAAATAGTGACTATAGGAATTACCA-GCAAAATGTG-3'; 133, 5'-TGATATCCTTAATGGTC-GTTTTACAACGTCGTGACTGGG-3'; 107, 5'-GACAT-CAGAGTCGACTGATGGCTCCACGCACGTTGTG-3'; intergenic region deletion: 152, 5'-CGAGAGTCGAC-

GAGCTAAGGTCTCACTATTTTCACAG-3'; 113, 5'-GT-GACCTTGCCAGAGACCCATGGTTAGCCCAATG-3'; 114 5'-AATGGGTCTCTGGCAAGTCCATAGCATT-ACCTGG-3'; and 151, 5'-GACATCAGAGTCGACTGA-CTCCTGCCAAGAAATCCTTCC-3'. The construction of the R2GFP shuttle vector was as described (12).
27. We thank N. Heintz and W. Yang for help with BAC technology, F. Isdell and M. Genova for help with flow cytometry, D. Dorsett for helpful discussions, and E. Besmer and members of the Nussenzweig lab for suggestions. Supported by NIH Medical Scientist Training Program grant GM07739, the Surdna Foundation, and the William Randolph Hearst Foundation (W.Y.); NIH (M.C.N. and R.R.H.); and the Howard Hughes Medical Institute (M.C.N.).

5 May 1999; accepted 14 July 1999

Control of the Terminal Step of Intracellular Membrane Fusion by Protein Phosphatase 1

C. Peters,¹ P. D. Andrews,² M. J. R. Stark,² S. Cesaro-Tadic,¹ A. Glatz,¹ A. Podtelejnikov,³ M. Mann,³ A. Mayer^{1*}

Intracellular membrane fusion is crucial for the biogenesis and maintenance of cellular compartments, for vesicular traffic between them, and for exo- and endocytosis. Parts of the molecular machinery underlying this process have been identified, but most of these components operate in mutual recognition of the membranes. Here it is shown that protein phosphatase 1 (PP1) is essential for bilayer mixing, the last step of membrane fusion. PP1 was also identified in a complex that contained calmodulin, the second known factor implicated in the regulation of bilayer mixing. The PP1-calmodulin complex was required at multiple sites of intracellular trafficking; hence, PP1 may be a general factor controlling membrane bilayer mixing.

Intracellular membrane fusion can be divided into distinct subreactions: priming, tethering and docking of the membranes, and subsequent mixing of the bilayers and contents (1). Most components identified so far, such as NSF (NEM-sensitive fusion protein), α -SNAP (soluble NSF attachment protein), SNAREs (SNAP receptors), Rab-like guanosine triphosphatases (GTPases) and their cofactors, and the LMA1 complex (low molecular weight activity), act in the early steps of intracellular membrane fusion, mediating recognition and association of the appropriate membranes. In contrast, there is little information about the transition from docking to bilayer mixing.

In the yeast *Saccharomyces cerevisiae*, the fusion of vacuoles to each other involves reactions that are identical to those that mediate fusion of intracellular membranes in

other eukaryotic cells (1). Vacuole fusion also requires an efflux of calcium from the vacuolar lumen (2), which is controlled by priming and docking of the vacuoles. The release of calcium into the cytosol results in a transient association of the cytosolic calcium-binding protein calmodulin with the vacuole membrane, which triggers the final events of bilayer and contents mixing. The final stage is also characterized by its sensitivity to certain low molecular weight compounds such as the serine-threonine phosphatase inhibitor microcystin LR, mastoparan, and guanosine 5'-O-(3'-thiotriphosphate) (3).

The target of microcystin LR is membrane-associated because microcystin LR inhibited vacuole fusion in the absence of cytosol (4). To identify the target of microcystin LR on yeast vacuolar membranes, we fractionated purified vacuole membranes by affinity chromatography with microcystin LR that was immobilized on Sepharose beads (5). In contrast to free microcystin LR, which forms covalent adducts with protein phosphatases (6), the immobilized form can associate with these enzymes noncovalently. Purified vacuolar membranes (7) were solubilized in detergent and passed over microcystin LR-

Sepharose (5). SDS-polyacrylamide gel electrophoresis (SDS-PAGE) analysis revealed that only one protein of ~35 kD could be specifically eluted from the Sepharose with free microcystin LR (Fig. 1A). Incubation of the solubilized membrane with free microcystin LR inhibited binding of the 35-kD protein to microcystin LR-Sepharose. Association of the other proteins was not completely blocked by free microcystin LR, and we regarded them as nonspecific. An excised region of the gel containing the 35-kD protein was degraded by trypsin (8), and the resulting peptide mixture was analyzed by high-accuracy matrix-assisted laser desorption/ionization (MALDI) mass spectrometry (9).

Eight peptide masses matched the calculated tryptic peptide masses of the yeast open reading frame YER133w (10) and identified the protein as protein phosphatase 1 (PP1). The involvement of PP1 in vacuole fusion was supported by the fact that affinity-purified antibodies to PP1 inhibited vacuole fusion in vitro (11) (Fig. 1B). Furthermore, purified yeast inhibitor 2 (12), a highly specific negative regulator of PP1 (13), inhibited vacuole fusion (Fig. 1C). Addition of purified recombinant PP1 (14) rescued the block to fusion caused by microcystin LR (Fig. 1D).

PP1 is an essential protein (15). To further examine the role of PP1 in fusion, we generated temperature-sensitive (ts) PP1 mutants (16). Vacuoles prepared from mutant strains that were grown at the permissive temperature (25°C) were fusion competent at 25°C (Fig. 2A). In contrast, short incubation of the vacuoles at the nonpermissive temperature (37°C) inhibited fusion. Vacuoles from wild-type yeast retained their fusion competence at 37°C. Inactivation of PP1 in the mutant strains by a temperature shift also disrupted vacuolar structure in vivo. At the nonpermissive temperature the vacuole disintegrated into small vesicles that aggregated (Fig. 2B). Under the same conditions, wild-type cells maintained a single large vacuole, as did the mutant cells at the permissive temperature. Overexpression of yeast inhibitor 2 in wild-type cells also caused vacuole fragmentation

¹Friedrich-Miescher-Laboratorium, Spemannstrasse 37-39, 72076 Tübingen, Germany. ²Department of Biochemistry, MSI/WTB Complex, University of Dundee, Dundee DD1 5EH, Scotland. ³Protein Interaction Laboratory, Department of Molecular Biology, University of Southern Denmark, Campusvej 55, 5230 Odense M, Denmark.

*To whom correspondence should be addressed. E-mail: andreas.mayer@tuebingen.mpg.de